scientific reports

Check for updates

OPEN

Partial microglial depletion and repopulation exert subtle but differential effects on amyloid pathology at different disease stages

L. H. D. Le[1], M. K. O'Banion[1] & A. K. Majewska[1,2]✉

Colony-stimulating factor-1-receptor (CSF1R) inhibitors have been widely used to rapidly deplete microglia from the brain, allowing the remaining microglia population to self-renew and repopulate. These new-born microglia are thought to be "rejuvenated" and have been shown to be beneficial in several disease contexts and in normal aging. Their role in Alzheimer's disease (AD) is thus of great interest as they represent a potential disease-modifying therapy. Here, we explored the differential effects of microglial depletion and repopulation during amyloid pathology progression using 5xFAD mice. We utilized the CSF1R inhibitor PLX3397 to induce microglial self-renewal and tracked microglia-plaque dynamics with in vivo imaging. We observed transient improvement in plaque burden on different timescales depending on the animal's age. While the improvement in plaque burden did not persist in any age group, renewing microglia during mid- to late-pathology might still be beneficial as we observed a potential improvement in microglial sensitivity to noradrenergic signaling. Altogether, our findings provide further insights into the therapeutic potential of microglial renewal in AD.

Microglia are the resident innate immune cells of the central nervous system (CNS). They play a key role in neurodevelopment and plasticity, as well as in the pathogenesis of a wide array of neurodevelopmental and neurodegenerative disorders[1–3]. In Alzheimer's disease (AD), genetic risk factors are disproportionately linked to immune receptors expressed by microglia[4–7], positioning these cells as important targets for disease-modifying therapies. However, in the chronic neuroinflammatory environment in AD, the role of microglia is complex. In fact, removal of microglia in AD mouse models via inhibition of colony-stimulating factor 1 receptor (CSF1R), which is critical for microglial survival and proliferation, reduced plaque formation when administered early[8,9] but not during advanced amyloid pathology, which is more translationally relevant. Additionally, while some studies have shown that late loss of microglia improved learning and memory, and lessened neuronal loss[10,11], others demonstrated that it also increased plaque-associated neuritic damage[12]. In the latter case, areas of plaque not covered by microglia were demonstrated to be more "diffuse", and their high affinity to Aβ1–42 aggregation created 'protofibrillar Aβ1–42 hotspots' that associated with a greater extent of axonal dystrophy[13]. These findings support an important role of microglia in forming a protective barrier enveloping amyloid plaque to limit neurotoxic effects of filamentous Aβ on surrounding neurons[13,14].

Rather than removing microglia, renewing them through depletion followed by repopulation presents another exciting strategy. Adult microglia are capable of rapidly replenishing their niche within 1 week after removal of CSF1R inhibitor, restoring their morphology and physiological functions[15–17]. In several injury models and in aging, repopulated microglia have been shown to be beneficial in promoting brain recovery[18–20] and reversing age-related neuronal deficits[21]. However, in the context of AD, we previously found no beneficial effects of microglial repopulation on either amyloid pathology nor cognitive function in aged transgenic mice harboring both amyloid and tau pathology[22]. On the other hand, early microglia renewal was suggested to partially rescue cognitive deficits by restoring the microglial homeostatic phenotype[23]. Here, we sought to delineate the dynamic effects of microglial depletion followed by repopulation on microglia function and Aβ plaque burden during different stages of amyloid pathology. We administered the CSF1R inhibitor PLX3397 (hereafter referred to

[1]Department of Neuroscience, Del Monte Institute for Neuroscience, University of Rochester, Rochester, NY, USA. [2]Center for Visual Science, University of Rochester, Rochester, NY, USA. ✉email: ania_majewska@urmc.rochester.edu

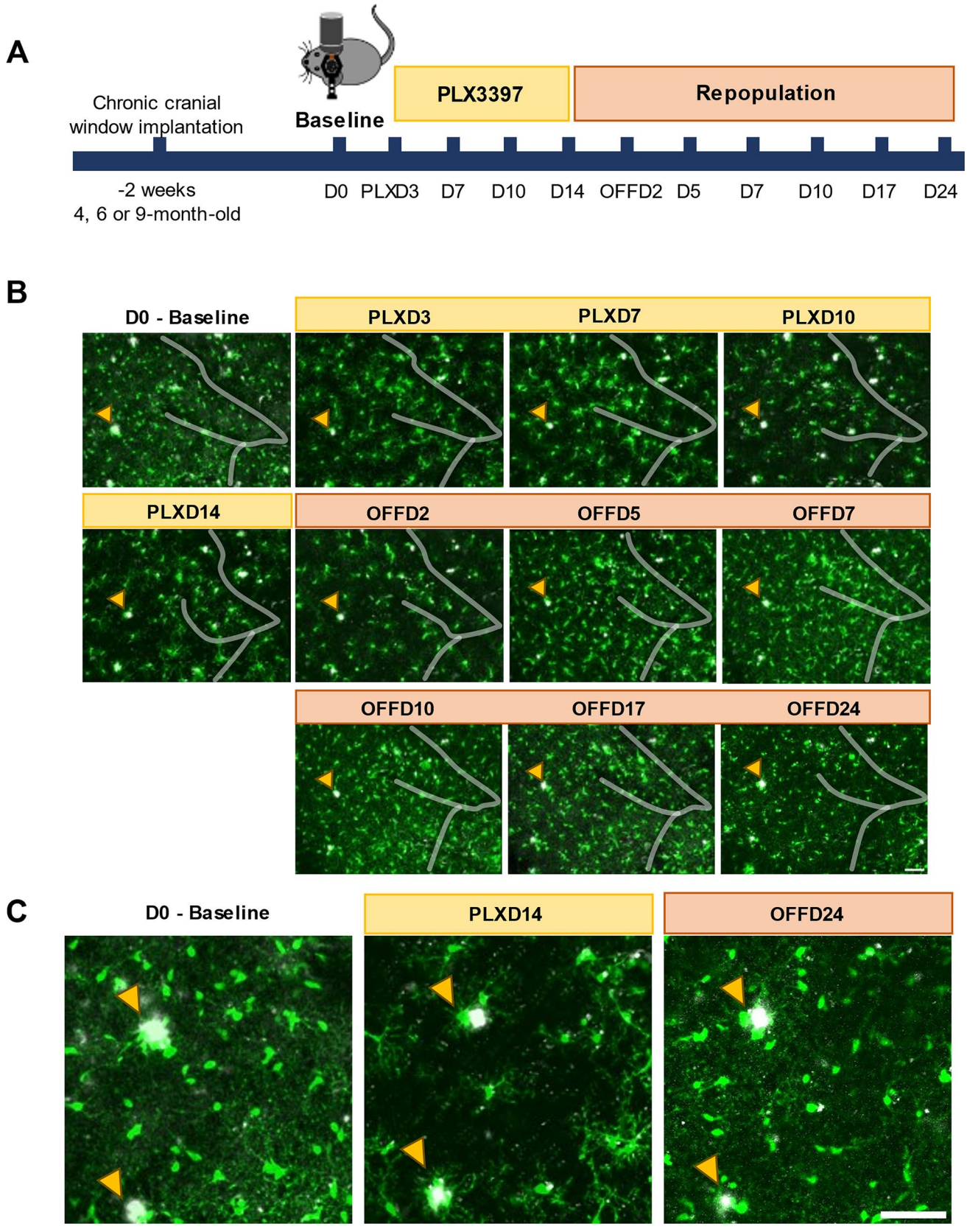

as PLX) in 5xFAD mice and tracked microglia-plaque dynamics with in vivo imaging. We revealed a transient improvement in plaque burden that occurred during either the depletion or repopulation period depending on the animal's age. Interestingly, while the improvement in plaque load did not persist long-term, repopulated microglia during mid-to-late pathology stages appeared to retain or increase their sensitivity to noradrenergic signaling, which is largely thought to be anti-inflammatory[24–33].

◀**Fig. 1**. Experimental paradigm. (**A**) In vivo imaging experimental timeline. CX3CR1$^{GFP/+}$(Control) and CX3CR1$^{GFP/+}$5xFAD$^{+/-}$(5xFAD) mice of 3 age groups (4, 6, and 9 months) were imaged at baseline (D0), during PLX treatment (4 timepoints), and after PLX discontinuation (6 timepoints). (**B**) Representative in vivo two-photon z-projected images across the entire depletion-repopulation timeline in a 9-month-old 5xFAD animal. Blood vasculature (outlined with semi-transparent white lines) was used as a gross landmark to consistently image the same area. Yellow arrow points to a large plaque that was stable across time. Scale bar = 50μm. (**C**) Zoomed-in representative in vivo two-photon z-projected images at D0 (baseline), PLXD14 (last day of PLX treatment) and OFFD24 (last timepoint) of the same animal in (**B**). Yellow arrows point to large plaques that were stable across time. Scale bar = 50μm.

Results

Tracking microglia-plaque dynamics in vivo during microglial depletion and repopulation

We utilized two-photon in vivo imaging to chronically track changes in microglia and plaques during microglial depletion and repopulation in primary sensory cortices of CX3CR1$^{GFP/+}$ 5xFAD and CX3CR1$^{GFP/+}$ littermate control mice at three different ages which correspond to early (4 months), mid (6 months) and late (9 months; when plaque load plateaus) phases of disease progression[34,35] (Fig. 1A–C). Similar to previous studies[11,17,22,23], we observed rapid and significant loss of microglia during PLX treatment in young (4 month) mice of both genotypes, along with a rapid repopulation which replenished the niche fully within 5 days after discontinuation of PLX (Supplementary Fig. 1A). In 6- and 9-month-old control mice, significant depletion required delivering a double dose of PLX mixed with Nutella, which led to partial depletion of microglia with an increase in the size of the remaining microglial somas (Supplementary Fig. 1C-F; see Methods). Cessation of PLX treatment allowed full microglial repopulation (Supplementary Fig. 1C, E). In 5xFAD mice, 2x PLX only depleted plaque-distal microglia, albeit to a lesser extent and with smaller increases in remaining microglial soma size than in control mice, while plaque-associated microglia number and soma size remained largely unchanged (Supplementary Fig. 1C–F).

Differential effects of PLX-induced microglia depletion-repopulation with age in 5xFAD mice

In 4-month-old 5xFAD mice that already had substantial cortical plaque load when PLX treatment began, amyloid pathology continued to develop throughout the course of imaging (Fig. 2A–C, orange lines). However, if plaques were largely absent on the first day of imaging (most common in male 5xFAD mice), they did not develop further during microglial depletion or repopulation (Fig. 2A–C, black lines). In fact, these animals had a similar plaque fraction (0.05%) at the start of imaging (4 months) and at the end (5.5 months), compared to 6-month-old mice which had a 10-fold higher plaque fraction (mean: 0.6%; 95% CI: 0.378–0.816). In the 6- and 9-month groups, data were normalized to the first time point, which was not possible at 4 months, due to the initial lack of plaques in the field of view in many of the animals. In 6-month-old 5xFAD mice, PLX treatment did not alter plaque pathology (Fig. 2D–F), however, plaque load decreased transiently in both number and overall area fraction in the early stages of microglial repopulation (Fig. 2D–F). Interestingly, in 9-month-old 5xFAD mice, amyloid pathology decreased transiently at the beginning of PLX treatment but not during repopulation (Fig. 2G–K).

Changes in plaque-associated microglia at 9 months in response to CSF1R inhibition

While plaque-associated microglia were not depleted and did not alter their soma size in response to PLX treatment, we wondered whether they underwent other morphological changes that could impact PLX-induced changes in plaque load. We found no differences in the area occupied by plaque-associated microglia (including both somas and processes) across the entire depletion-repopulation time course in 6-month-old mice (Fig. 3A). However, we observed a significant increase in plaque-associated microglia area at the beginning of PLX treatment in 9-month-old mice (Fig. 3B), a time during which plaque load was reduced in these mice (Fig. 2G–I). This increase in plaque-associated microglia area during PLX treatment correlated with the observed reduction in plaque load but did not correlate with depletion rate of plaque distal microglia (Fig. 3C–E).

Assessment of the responsiveness of repopulated microglia to β2AR stimulation

Finally, we investigated whether repopulated microglia altered their sensitivity to noradrenergic signaling, which causes microglia to retract their processes by activating microglial β2 adrenergic receptors (β2ARs)[36,37], an effect we recently reported to decrease with age[38]. In 4- and 6-month-old animals, microglia retracted their process to the same extent in response to administration of the β2AR agonist, clenbuterol, across the imaging timeline (Fig. 4D-I). Interestingly, in 9-month-old mice, microglia in the repopulation phase in control and 5xFAD mice appeared to be more sensitive to clenbuterol than before depletion, although the effect was not statistically significant (Fig. 4J-L).

Discussion

In this study, we revealed differential effects of microglia depletion and repopulation as a function of amyloid pathology. We observed transient improvement in plaque burden on different timescales in 6 vs. 9-month-old mice. Additionally, if partial forced turnover of microglia occurred prior to plaque deposition in 4-month-old mice, plaque formation appeared to be delayed.

Microglia downregulate their *Csf1r* gene expression with age[39] which likely accounts for the need for an increased dose of PLX to achieve depletion in older cohorts in this study. In addition, similar to previous reports[22,23], plaque-associated microglia were resistant to even the increased dose of PLX, as these microglia

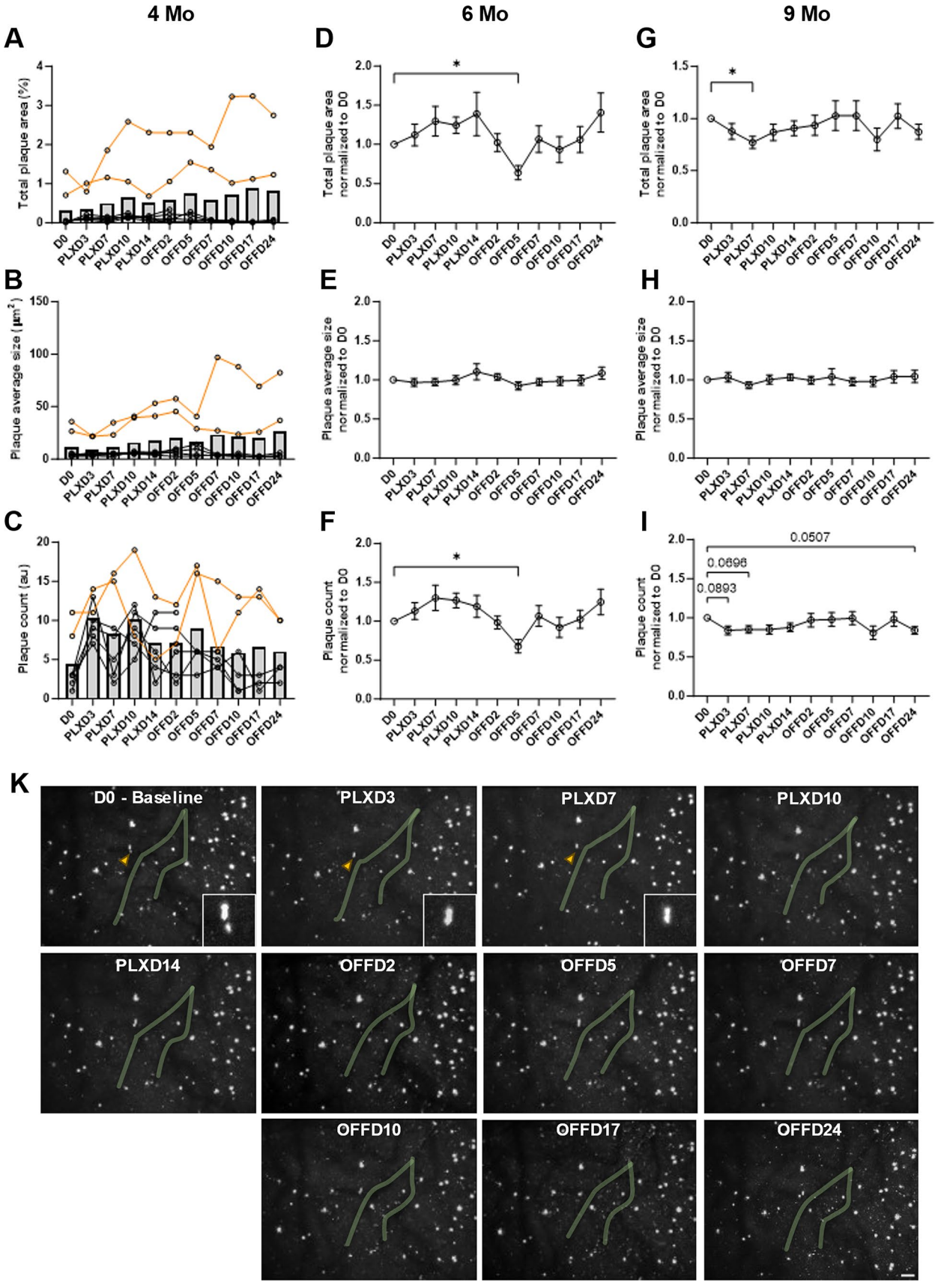

express significantly lower levels of *Csf1r* compared to plaque-distal microglia[40]. We did observe a transient morphological change (likely due to an increase in process thickness, since no change in soma size was detected) at the beginning of PLX treatment in 9 month old mice, suggesting a reactive state[41] that could result in plaque clearance, explaining the concurrent transient reduction in plaque burden. This suggests that brain-wide CSF1R

◀**Fig. 2**. PLX-induced microglia depletion-repopulation differentially impacted plaque load with age in 5xFAD mice. (**A**, **D**, **G**) Plaque area fraction before, during, and after PLX treatment presented as % area in the 4-month group (**A**), and normalized to D0 in the 6-month (**D**) and 9-month (**G**) groups. Each line in A represents an individual animal. Orange lines represent animals with substantial plaque deposition (n = 2 females) while black lines represent animals with relatively little plaque at D0 (n = 5; 4 males, 1 female; at D0, 3 at OFFD24). (**B**, **E**, **H**) Average size of plaque before, during, and after PLX treatment presented as absolute number (μm^2) in the 4-month group (**B**), and normalized to D0 in the 6-month (**E**) and 9-month (**H**) groups. Each line in **B** represents an individual animal, color-coded as in **A**. (**C**, **F**, **I**) Total number of plaques in the field of view before, during, and after PLX treatment presented as the absolute number in the 4-month group (**C**), and normalized to D0 in the 6-month (**F**) and 9-month (**I**) groups. Each line in **C** represents an individual animal, color-coded as in **A**. (**K**) Representative in vivo two-photon z-projected images showing plaque load in a 9-month-old 5xFAD animal during depletion-repopulation. While most of the large plaques were stable, the yellow arrow points to a small plaque that was cleared during the first few days of PLX treatment. Blood vasculature (outlined with semi-transparent green lines) was used as a gross landmark to consistently image the same area. Enlarged insets of this region are shown for D0, PLXD3 and PLXD7. Scale bar = 50μm. Sample size for each age group is as follows: 4-month: n = 7 at D0 and 5 at OFFD24; 6-month: n = 13 at D0 and 8 at OFFD24; 9-month: n = 12 at D0 and 8 at OFFD24. Notice that not all animals could be imaged for the entire timeline. One-way ANOVA with Dunnett's post-hoc correction; $^*p < 0.05$.

inhibition may initially alter the functional state of plaque-associated microglia and ameliorate advanced amyloid pathology. The fact that this effect was only observed at older ages when amyloid pathology was advanced, implies that even though plaque-associated microglia significantly downregulated their homeostatic markers and *Csf1r* expression at early in the disease[38,40], these microglia may undergo further phenotypical changes in response to aging and amyloid deposition, which may act synergistically to produce the observed transient morphological change in plaque-associated microglia during CSF1R inhibition.

If started before the onset of pathology, microglia repopulation seemed to limit or delay plaque deposition in 4-month-old mice, aligning with previous reports on the benefits of depleting microglia early[8,9]. Thus, disease-modifying effects may differ by brain area because of the differential degree of amyloid pathology. Moreover, partial depletion of microglia at this age together with delayed plaque formation might help curb the rapid proliferation of microglia in response to Aβ aggregates that leads to microglial replicative senescence[42].

In addition, renewing microglia may be beneficial in maintaining microglial responsiveness to β2AR stimulation which declines with age[38], but which we have recently shown to limit AD-related pathology[38]. Noradrenergic signaling has been well established as a potent anti-inflammatory regulator for microglia using primary cultures[24–26]. In microglia in vivo, activation of the Gs-coupled receptor β2AR leads to a downstream increase in cyclic AMP (cAMP), driving the collapse of large processes through rearrangement of the cytoskeleton[43], causing less surveillance activity and promoting a less immune-vigilant functional state[36,37]. We have found that 5xFAD microglia downregulate *β2AR* progressively with amyloid pathology[38], concurrent with their downregulation of *Csf1r* expression[40], suggestive of a shift toward a reactive phenotype in which microglia become resistant to CSF1R inhibition and progressively less responsive to noradrenergic signaling. Whether this phenotype may enhance the protective barrier function of microglia at plaques via the shift from CSF1R-dependent towards more CSF1R-independent survival mechanisms or contribute to the chronic inflammatory environment via increasing immune reactivity, or the combination of both, remains to be determined. It is important to note that in the 6-month-old age group where mice were 7.5 months at the last imaging timepoint, close to the 9-month mark where microglia no longer respond to β2AR stimulation, repopulated microglia still retracted their processes under β2AR stimulation. In 9-month-old mice, there was a trend towards increased responsiveness in repopulated microglia. Whether this maintained or improved responsiveness is long lasting is an open question as the on-going neuroinflammatory environment may shift repopulated microglia to a pre-depletion functional state[23,44,45].

Taken together, our findings offer a dynamic look at the effects of microglial replacement at different stages of amyloid pathology and provide further insights into the therapeutic potential of this approach.

Methods

Experimental animals

All animal procedures were reviewed and approved by the University Committee on Animal Resources of the University of Rochester Medical Center and performed according to the Institutional Animal Care and Use Committee and guidelines from the National Institute of Health (NIH), and in accordance with the ARRIVE guidelines. Animals were housed in a 12-hour light/12-hour dark cycle with ad libitum access to standard rodent chow and water. Male and female B6.Cg-Tg(APPSwFlLon, PSEN1*M146L*L286V)6799Vas/Mmjax mice (5xFAD[34]), were obtained from JAX (stock no. 034848, donated to the MMRRC at JAX by Robert Vassar, Ph.D., Northwestern University) and maintained at the University of Rochester vivarium. For all experiments in this study, 5xFAD mice were crossed with homozygous CX3CR1-GFP reporter mice (JAX stock no. 005582[46]), to generate $CX3CR1^{GFP/+}$ 5xFAD and $CX3CR1^{GFP/+}$ littermate controls. All mice were derived from and maintained on a C57BL/6J background.

Microglia depletion with PLX3397

To compare the efficacy of PLX3397-incorporated chow diet and PLX3397-incorporated Nutella, mice received either a chow diet (AIN-76 A-D1001, Research Diets) containing 290 mg/kg PLX3397 (Chemgood) ad libitum,

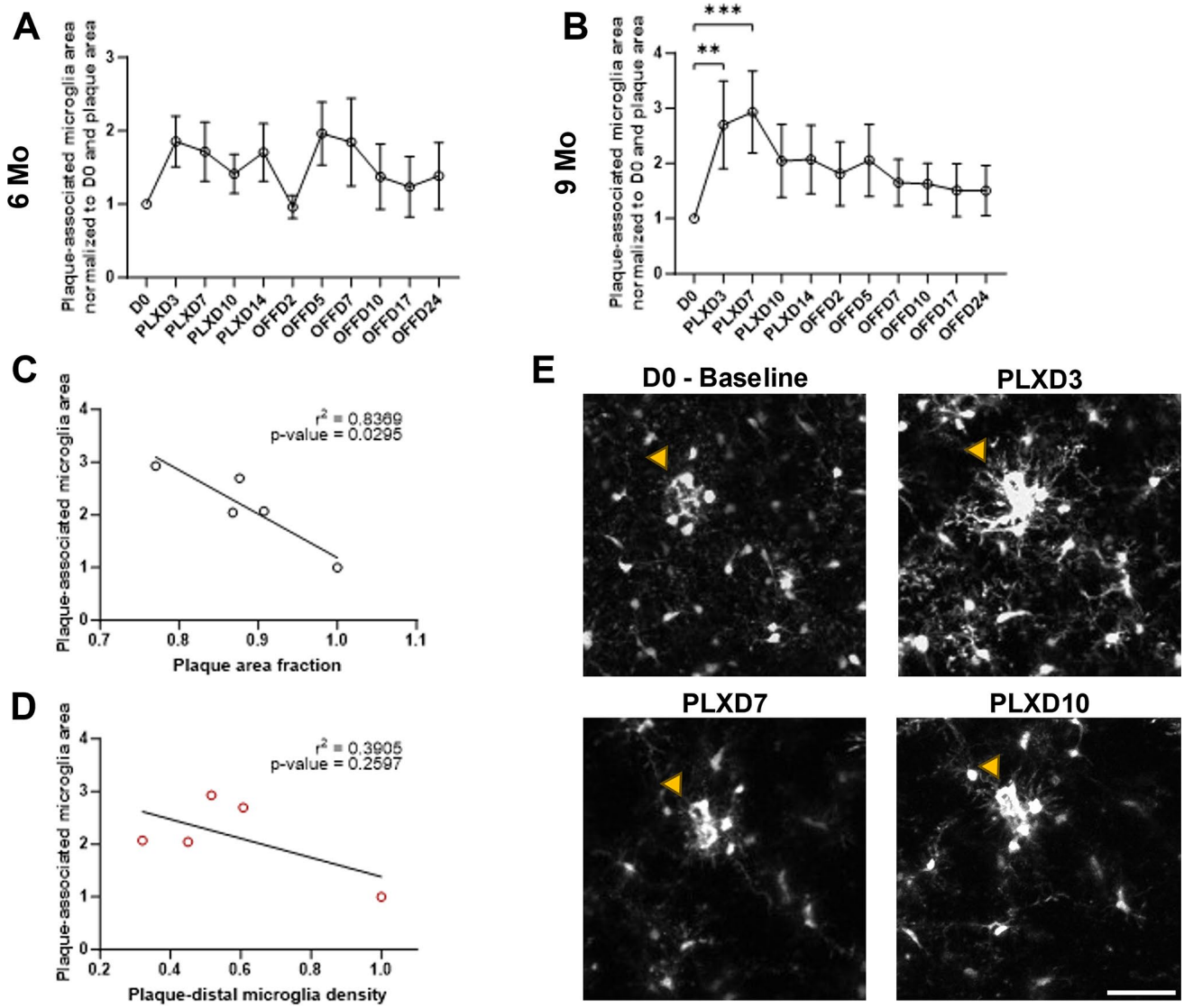

Fig. 3. Plaque-associated microglia at 9 months enlarged their process area upon PLX treatment. (**A**–**B**) Plaque-associated microglia area across the depletion-repopulation period as normalized to D0 and plaque load in all animals at 6 months (**A**) and 9 months (**B**). (**C**–**D**) During the depletion period in the 9-month group, plaque-associated microglia area negatively correlated with plaque load (**C**) but did not correlate with degree of depletion of plaque-distal microglia (**D**). (**E**) Representative in vivo two-photon z-projected images showing microglia morphological changes in a 9-month-old 5xFAD animal during the depletion period. Yellow arrow pointing to enlarged microglial processes after 3 days of PLX treatment. Scale bar = 50μm. Sample size as in Fig. 2. Since most of the 4-month-old 5xFAD did not develop enough amyloid pathology, they were excluded from this analysis. One-way ANOVA with Dunnett's post-hoc correction; $^{**}p < 0.01$, $^{***}p < 0.001$ (**A**, **B**). Simple linear regression analysis (**C**, **D**).

or a comparable dose of PLX3397 mixed with Nutella (1:1000 concentration, 1–1.25 g of mixture consumed/mouse/day)[47,48] given orally on polystyrene Petri dishes placed inside home cages, to deplete microglia for 7 days. After confirming depletion of microglia with voluntary oral ingestion of PLX3397-incorporated Nutella (Supplementary Fig. 2), this method was used for all other experiments in this study. While PLX3397 chow diet has a relatively short shelf life, the PLX3397-Nutella mixture can be prepared immediately prior to administration and the PLX3397compound can be safely stored long-term in − 20 °C freezer.

Due to the high resistance of aged 5xFAD microglia to CSF1R inhibition using the standard dose of PLX3397[15] (Supplementary Fig. 3), mice that were 6 or 9 months at the start of the experiments were given 2x PLX3397 (1:500 PLX3397 in Nutella) to achieve higher degree of depletion.

Pharmacological agents

Fentanyl cocktail comprised fentanyl (0.05 mg/kg), midazolam (5.0 mg/kg) and dexmedetomidine (0.5 mg/kg) premixed in saline and was injected intraperitoneally (i.p.) once for anesthesia prior to each two-photon imaging

session that collected XYZT stacks, which lasted 1.5 h. For each two-photon imaging session collecting just XYZ stacks, which lasted 15–30 min, a 50% dose of the fentanyl cocktail was used to avoid anesthetizing animals for longer than necessary. The loss of righting reflex was used to make sure the animal was deeply anesthetized for the time of the imaging session in both cases.

Methoxy-X04 (MX04, Tocris Biosciences), a brain-permeable fibrillar Aβ fluorescent marker[49,50], was dissolved in DMSO, then mixed in propylene glycol and 1x PBS, and was injected i.p. at 4 mg/kg 24 h prior to the first imaging session to label Aβ senile plaques. Mice were given additional doses once every 5 days (i.p., 1 mg/kg) for subsequent imaging sessions[49,50].

To stimulate central β2ARs, nadolol (10 mg/kg i.p.; Sigma, 42200-33-9; brain impermeable β2AR antagonist) and clenbuterol (1 mg/kg i.p.; Sigma, 21898-19-1; brain permeable β2AR agonist) were administered for two-photon imaging. Both nadolol and clenbuterol were dissolved in saline. At least 1 h prior to being imaged, mice were pre-dosed with the brain-impermeant β2AR antagonist nadolol to account for peripheral effects of clenbuterol on cardiorespiratory systems during imaging[36].

Cranial window surgery

Cranial window preparation was performed as described previously[17,36,38]. Animals were anesthetized using the fentanyl cocktail (i.p.) during the cranial window implantation surgical procedure. Body temperature was maintained at 37 °C with a heating pad and the animal's eyes were protected with lubricant ointment. All surgical procedures adhered to aseptic technique. Mice were fixed in a stereotaxic frame; hair was removed, and the skull was exposed through a scalp incision. A 3-mm biopsy punch (Integra) was then used to create a circular score on the skull over V1. A 0.5-mm drill bit (FST) was used to then drill through the skull for the craniotomy, tracing the 3-mm score. The 3-mm-diameter skull bone was gently lifted off, maintaining the dura mater underneath intact. A 5-mm coverslip attached to a 3-mm coverslip (Warner Instruments) by UV glue (Norland Optical Adhesive, Norland) was then slowly lowered into the craniotomy (3-mm side down). The coverslip was carefully secured with C&B Metabond dental cement (Parkell). A custom headplate produced by emachine shop (http://www.emachineshop.com) (designs courtesy of the Mriganka Sur laboratory, Massachusetts Institute of Technology) was then secured onto the skull with the same dental cement, the rest of which was used to cover any exposed skull and seal the incision site. Mice were administered slow-release buprenex (5 mg/kg subcutaneously for 72 h) and carprofen (5 mg/kg, i.p. every 24 h) and monitored for 72 h postoperatively.

Two-photon microscopy image acquisition and analysis

A custom two-photon laser-scanning microscope was used for in vivo imaging (Ti: Sapphire, Mai-Tai, Spectra Physics; modified Fluoview confocal scan head, 20x water immersion objective lens, 0.95 NA, Olympus). Excitation for fluorescence imaging was achieved with 100-fs laser pulses (80 MHz) at 920 nm for GFP and 770 nm for MX04 with a power of ~40–50 mW measured at the sample. Fluorescence was detected using a photomultiplier tube with a 580/180 bandpass filter (GFP, microglia) and 460/80 filter (MX04-labeled plaque).

Mice were anesthetized with the fentanyl cocktail for imaging. During and post-imaging, body temperature was maintained at 37 °C with a heating pad and the animal's eyes were protected with lubricant ointment. Z-stacks were acquired with z-step size of 2 µm at 1x and 1.5x digital zoom for measurements of plaque load and microglia-plaque interaction, respectively. For assessment of microglia dynamics, time-lapse imaging was carried out at 5 min intervals over 1.5 h, 45–60 µm z-stack depth at 1 µm step size at each time point, 4x digital zoom. For β2AR stimulation, clenbuterol was administered 30 min into the imaging session, allowing for intra-animal comparisons of pre- (first 30 min) and post- (last 30 min) stimulation to assess the retraction of processes in response to β2AR stimulation. During the baseline imaging session, before depletion, animals also underwent the same procedure where clenbuterol was substituted with saline to assess the contributions of bleaching and injection to the retraction response. To limit peripheral effects of clenbuterol, nadolol was given 1 h before the imaging session. For repeated imaging, blood vessels were used as gross landmarks and stable microglia were also used as fine landmarks to re-identify the correct region for imaging. All imaging time points are presented in Fig. 1. Image analysis was done offline using ImageJ FIJI (NIH), Ilastik[51] and MATLAB with custom algorithms. All custom-made scripts are available at https://github.com/majewska-lab.

For assessment of changes in plaque load and microglia-plaque interaction prior to, during, and after PLX treatment, all images were first subjected to within-stack alignment to correct for XY drift, then for each animal, the same number of z-slices representing the same area in both XY location and Z-depth was chosen across all imaging sessions. Images were subjected to preprocessing steps including despeckle, gaussian smoothing, and background subtraction. It should be noted that due to technical difficulties such as degradation in quality of imaging of specific brain areas and the brain's inherent volumetric changes, a few imaging sessions (approximately less than 10%) were carried out in a similar location instead of the exact area from the previous session. For plaque load analysis, maximum z-projections (1x digital zoom) were thresholded and binarized using semi-automated ImageJ's Yen thresholding algorithm. Plaque area fraction, total number of plaques and average plaque size were reported using automated ImageJ's analyze particles function with a cut-off size of 30 μm^2. For visualization purposes, all data collected from 6- and 9-month groups were normalized to measurements at baseline (D0, Fig. 1). Because at 4 months, male 5xFAD mice have not yet developed substantial or stable plaque load in the superficial cortex accessible for imaging (outer layer II/III), data were not normalized for these mice. For plaque-microglia interaction analysis, microglia and plaque z-stacks (1.5x digital zoom) were subjected to automated ImageJ's Triangle and Yen thresholding methods, respectively. The plaque z-stacks were dilated by 15 µm then multiplied with the microglia z-stacks to calculate the number of colocalized signal pixels as plaque-associated microglia area. Analysis of plaque-associated microglia on z-stacks allowed for the capture of all microglia associated with plaques in the z-direction and avoid overlapping caused by max projection, although some microglia at the top and bottom of the plaque were likely not captured. The plaque-associated microglia

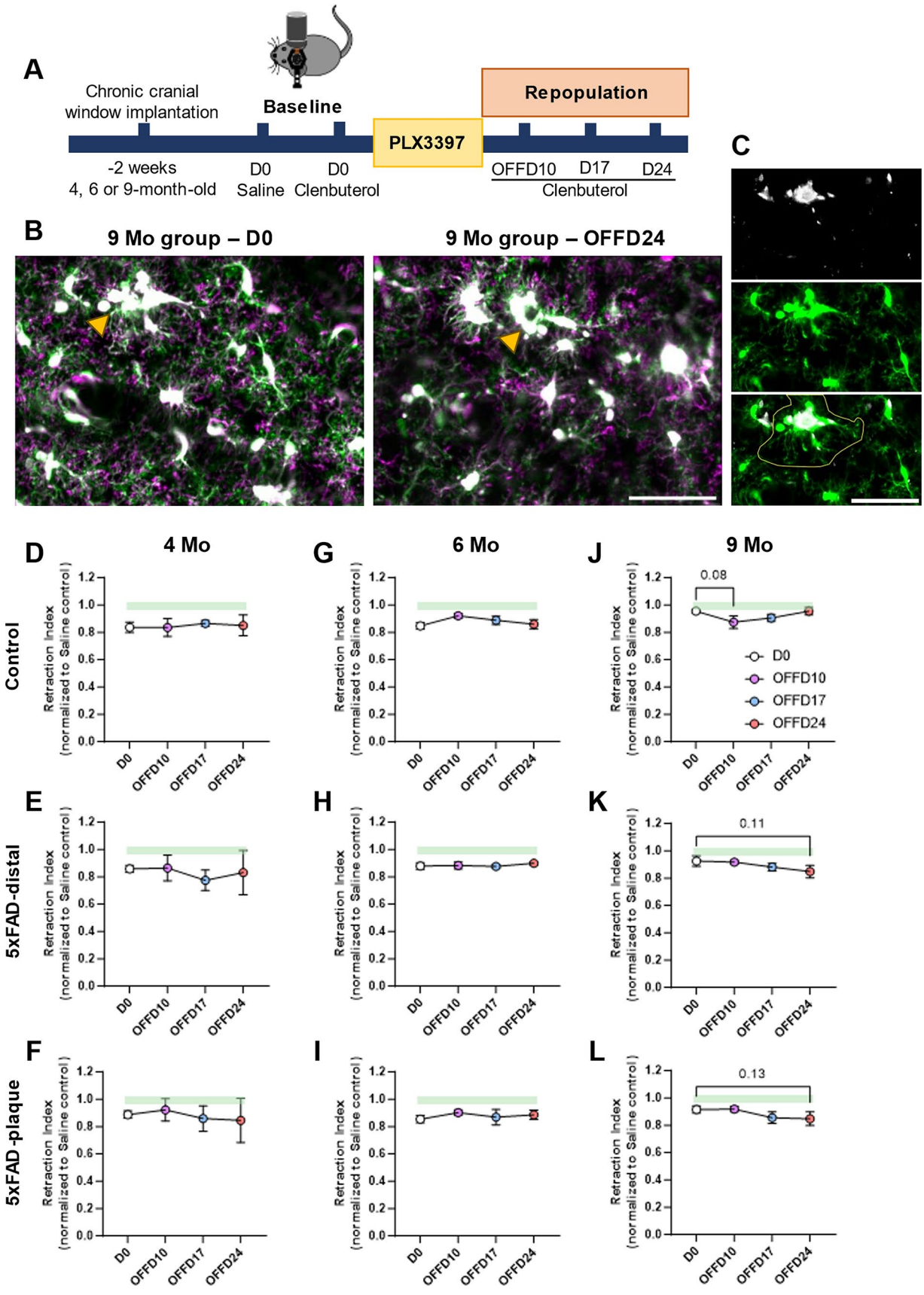

area for each imaging session was normalized to the plaque area measured from the same session, and then to the plaque-associated microglia area at baseline (D0, Fig. 1).

For automated detection of microglia somas, the image classification and segmentation software, Ilastik[51], was used. Isolation of plaque-associated microglia was done similarly to the process described above, except the

◀**Fig. 4**. Assessment of repopulated microglia responsiveness to β2AR stimulation. (**A**) In vivo imaging experimental timeline, modified from Fig. 1A to show timepoints with microglial β2AR stimulation. Baseline microglial response to saline and clenbuterol treatment were collected (D0) for all control and 5xFAD mice of 3 age groups (4, 6, and 9 months). Animals were subsequently imaged with clenbuterol treatment at OFFD10, 17 and 24. For all treatments, imaging was carried out for 30 minutes (pre-treatment). Saline or clenbuterol were then applied, followed by 15 minutes intermission, and imaging continued for 30 minutes (post-treatment). (**B**) Representative in vivo two-photon time projected images from 9-month-old 5xFAD mice at baseline (D0) and 24 days post PLX (OFFD24). Images obtained before treatment (pre-treatment) are shown in magenta and superimposed on images obtained after clenbuterol injection (post-treatment) which are shown in green. Notice the increased number of magenta (retracted) pixels in relation to green (extended) pixels at OFFD24. An example of plaque-associated microglia in each image is marked with a yellow arrowhead. Scale bar = 50μm. (**C**) Representative in vivo two-photon images showing the selection and isolation of plaque-associated microglia (outlined in yellow). Plaques are shown in the top panel, microglia in the middle panel and the merged image is shown in the bottom panel. Scale bar = 50μm. (**D**–**L**) Quantification of the normalized retraction index on D0 and weekly from D10 post PLX in control mice (**D**: 4 months; **G**: 6 months; **J**: 9 months), 5xFAD mice for plaque-distal (**E**: 4 months; **H**: 6 months; **K**: 9 months) or plaque-associated (**F**: 4 months; **I**: 6 months; **L**: 9 months) microglia. The retraction index is defined as the area of the image covered by microglia post-clenbuterol administration divided by this area pre-clenbuterol administration, and is then normalized to the retraction index obtained in response to saline treatment at D0 (averages shown in green bars) to account for bleaching artifacts. Sample size as in Fig. 2. One-way ANOVA with Dunnett's post-hoc correction.

microglia z-stacks were not thresholded. The outlines of 15 μm-dilated plaques were used to crop out plaque-associated microglia. Three labels were used to train for pixel classification including microglial soma, processes, and background. Microglial processes were demarcated for training to provide contrast for better soma detection. Approximately 6% of all 1.5x microglia images representing microglia at baseline, during and after PLX treatment were manually annotated for approximately 25–50% area of the image. After sufficient training, appropriate thresholding and size exclusion criteria were applied for batch object classification of microglial somas.

For assessment of microglia dynamics, all images were subjected to preprocessing steps in ImageJ as previously described[36,52]. Microglia physically touching plaques (as observed by overlaying the microglia channel over the plaque channel) were defined as plaque-associated microglia and were manually isolated (Fig. 4C). For automated detection of microglial processes, Ilastik[51] was used. To train for pixel classification, microglia processes and somas were manually traced. Appropriate thresholding and size exclusion criteria were applied for object classification. Outputs of microglial processes were binarized in ImageJ for microglia surveillance analysis. Microglia surveillance represented how much of the parenchyma microglia survey over time. The surveillance index was calculated by dividing the number of binarized microglia pixels by all pixels in the maximum projection of all timepoints. To assess the effects of β2AR stimulation, the retraction index was calculated as the ratio between post and pre-treatment surveillance index. Saline treatments were only conducted once prior to PLX treatment of all animals and were represented in Fig. 4 as light green bars. The surveillance fraction of clenbuterol-treated microglia at each time point was then normalized to the surveillance fraction of saline-treated microglia at baseline to obtain the normalized retraction index.

Statistical analysis

Data organization and summary were carried out in RStudio with R v4. All statistical analyses and graphing were performed in Graphpad Prism v10. Comparisons across all imaging sessions were done using one-way or two-way ANOVA with appropriate post-hoc correction. Detailed statistics are provided in the appropriate figure legends. All data points represent individual animal averages and are presented as mean ± SEM.

Data availability

The raw data supporting the findings of this study and training models for image analysis will be made available from the corresponding author upon reasonable request from any qualified researcher.

Received: 11 September 2024; Accepted: 29 November 2024
Published online: 28 December 2024

References

1. Song, W. M. & Colonna, M. The identity and function of microglia in neurodegeneration. *Nat. Immunol.* **19** (10), 1048–1058 (2018).
2. Heneka, M. T. et al. Neuroinflammation in Alzheimer's disease. *Lancet Neurol.* **14** (4), 388–405 (2015).
3. Butovsky, O. & Weiner, H. L. Microglial signatures and their role in health and disease. *Nat. Rev. Neurosci.* **19** (10), 622–635 (2018).
4. Hollingworth, P. et al. Common variants at ABCA7, MS4A6A/MS4A4E, EPHA1, CD33 and CD2AP are associated with Alzheimer's disease. *Nat. Genet.* **43** (5), 429–435 (2011).
5. Naj, A. C. et al. Common variants at MS4A4/MS4A6E, CD2AP, CD33 and EPHA1 are associated with late-onset Alzheimer's disease. *Nat. Genet.* **43** (5), 436–441 (2011).
6. Guerreiro, R. et al. TREM2 variants in Alzheimer's disease. *N Engl. J. Med.* **368** (2), 117–127 (2013).
7. Jonsson, T. et al. Variant of TREM2 associated with the risk of Alzheimer's disease. *N Engl. J. Med.* **368** (2), 107–116 (2013).

8. Spangenberg, E. et al. Sustained microglial depletion with CSF1R inhibitor impairs parenchymal plaque development in an Alzheimer's disease model. *Nat. Commun.* **10** (1), 3758 (2019).
9. Sosna, J. et al. Early long-term administration of the CSF1R inhibitor PLX3397 ablates microglia and reduces accumulation of intraneuronal amyloid, neuritic plaque deposition and pre-fibrillar oligomers in 5XFAD mouse model of Alzheimer's disease. *Mol. Neurodegener.* **13** (1), 11 (2018).
10. Dagher, N. N. et al. Colony-stimulating factor 1 receptor inhibition prevents microglial plaque association and improves cognition in 3xTg-AD mice. *J. Neuroinflammation.* **12**, 139 (2015).
11. Spangenberg, E. E. et al. Eliminating microglia in Alzheimer's mice prevents neuronal loss without modulating amyloid-beta pathology. *Brain* **139** (Pt 4), 1265–1281 (2016).
12. Casali, B. T. et al. Microglia depletion rapidly and reversibly alters amyloid pathology by modification of plaque compaction and morphologies. *Neurobiol. Dis.* **142**, 104956 (2020).
13. Condello, C. et al. Microglia constitute a barrier that prevents neurotoxic protofibrillar Abeta42 hotspots around plaques. *Nat. Commun.* **6**, 6176 (2015).
14. Yuan, P. et al. TREM2 haplodeficiency in mice and humans impairs the Microglia barrier function leading to decreased amyloid compaction and severe axonal dystrophy. *Neuron* **92** (1), 252–264 (2016).
15. Elmore, M. R. et al. Colony-stimulating factor 1 receptor signaling is necessary for microglia viability, unmasking a microglia progenitor cell in the adult brain. *Neuron* **82** (2), 380–397 (2014).
16. Huang, Y. et al. Repopulated microglia are solely derived from the proliferation of residual microglia after acute depletion. *Nat. Neurosci.* **21** (4), 530–540 (2018).
17. Mendes, M. S. et al. The role of P2Y12 in the kinetics of microglial self-renewal and maturation in the adult visual cortex in vivo. *Elife*, 10. (2021).
18. Li, X. et al. Microglial replacement in the aged brain restricts neuroinflammation following intracerebral hemorrhage. *Cell. Death Dis.* **13** (1), 33 (2022).
19. Rice, R. A. et al. Microglial repopulation resolves inflammation and promotes brain recovery after injury. *Glia* **65** (6), 931–944 (2017).
20. Willis, E. F. et al. Repopulating microglia promote brain repair in an IL-6-dependent manner. *Cell* **180** (5), 833–846e16 (2020).
21. Elmore, M. R. P. et al. Replacement of microglia in the aged brain reverses cognitive, synaptic, and neuronal deficits in mice. *Aging Cell.* **17** (6), e12832 (2018).
22. Karaahmet, B. et al. Repopulated microglia induce expression of Cxcl13 with differential changes in tau phosphorylation but do not impact amyloid pathology. *J. Neuroinflammation.* **19** (1), 173 (2022).
23. Wang, W. et al. Microglial repopulation reverses cognitive and synaptic deficits in an Alzheimer's disease model by restoring BDNF signaling. *Brain Behav. Immun.* **113**, 275–288 (2023).
24. Mori, K. et al. Effects of norepinephrine on rat cultured microglial cells that express alpha1, alpha2, beta1 and beta2 adrenergic receptors. *Neuropharmacology* **43** (6), 1026–1034 (2002).
25. Markus, T. et al. beta-adrenoceptor activation depresses brain inflammation and is neuroprotective in lipopolysaccharide-induced sensitization to oxygen-glucose deprivation in organotypic hippocampal slices. *J. Neuroinflammation.* **7**, 94 (2010).
26. Farber, K., Pannasch, U. & Kettenmann, H. Dopamine and noradrenaline control distinct functions in rodent microglial cells. *Mol. Cell. Neurosci.* **29** (1), 128–138 (2005).
27. Heneka, M. T. et al. Locus ceruleus controls Alzheimer's disease pathology by modulating microglial functions through norepinephrine. *Proc. Natl. Acad. Sci. USA.* **107** (13), 6058–6063 (2010).
28. Heneka, M. T. et al. Locus ceruleus degeneration promotes Alzheimer pathogenesis in amyloid precursor protein 23 transgenic mice. *J. Neurosci.* **26** (5), 1343–1354 (2006).
29. Kalinin, S. et al. Noradrenaline deficiency in brain increases beta-amyloid plaque burden in an animal model of Alzheimer's disease. *Neurobiol. Aging.* **28** (8), 1206–1214 (2007).
30. Kalinin, S. et al. The noradrenaline precursor L-DOPS reduces pathology in a mouse model of Alzheimer's disease. *Neurobiol. Aging.* **33** (8), 1651–1663 (2012).
31. Ardestani, P. M. et al. Modulation of neuroinflammation and pathology in the 5XFAD mouse model of Alzheimer's disease using a biased and selective beta-1 adrenergic receptor partial agonist. *Neuropharmacology* **116**, 371–386 (2017).
32. Evans, A. K. et al. Beta-adrenergic receptor antagonism is proinflammatory and exacerbates neuroinflammation in a mouse model of Alzheimer's Disease. *Neurobiol. Dis.* **146**, 105089 (2020).
33. Branca, C. et al. Administration of a selective beta2 adrenergic receptor antagonist exacerbates neuropathology and cognitive deficits in a mouse model of Alzheimer's disease. *Neurobiol. Aging.* **35** (12), 2726–2735 (2014).
34. Oakley, H. et al. Intraneuronal beta-amyloid aggregates, neurodegeneration, and neuron loss in transgenic mice with five familial Alzheimer's disease mutations: Potential factors in amyloid plaque formation. *J. Neurosci.* **26** (40), 10129–10140 (2006).
35. Forner, S. et al. Systematic phenotyping and characterization of the 5xFAD mouse model of Alzheimer's disease. *Sci. Data.* **8** (1), 270 (2021).
36. Stowell, R. D. et al. Noradrenergic signaling in the wakeful state inhibits microglial surveillance and synaptic plasticity in the mouse visual cortex. *Nat. Neurosci.* **22** (11), 1782–1792 (2019).
37. Liu, Y. U. et al. Neuronal network activity controls microglial process surveillance in awake mice via norepinephrine signaling. *Nat. Neurosci.* **22** (11), 1771–1781 (2019).
38. Le, L. et al. Noradrenergic signaling controls Alzheimer's disease pathology via activation of microglial beta2 adrenergic receptors. *bioRxiv*, (2023).
39. Pan, J. et al. Transcriptomic profiling of microglia and astrocytes throughout aging. *J. Neuroinflammation.* **17** (1), 97 (2020).
40. Keren-Shaul, H. et al. A unique microglia type associated with restricting development of Alzheimer's disease. *Cell* **169** (7), 1276–1290e17 (2017).
41. Kettenmann, H. et al. Physiology of microglia. *Physiol. Rev.* **91** (2), 461–553 (2011).
42. Hu, Y. et al. Replicative senescence dictates the emergence of disease-associated microglia and contributes to Abeta pathology. *Cell. Rep.* **35** (10), 109228 (2021).
43. Bernier, L. P. et al. Nanoscale surveillance of the brain by microglia via cAMP-regulated filopodia. *Cell. Rep.* **27** (10), 2895–2908e4 (2019).
44. Gratuze, M. et al. Activated microglia mitigate Abeta-associated tau seeding and spreading. *J. Exp. Med.*, **218**(8). (2021).
45. O'Neil, S. M. et al. Forced turnover of aged microglia induces an intermediate phenotype but does not rebalance CNS environmental cues driving priming to immune challenge. *Acta Neuropathol. Commun.* **6** (1), 129 (2018).
46. Jung, S. et al. Analysis of fractalkine receptor CX(3)CR1 function by targeted deletion and green fluorescent protein reporter gene insertion. *Mol. Cell. Biol.* **20** (11), 4106–4114 (2000).
47. Cangalaya, C. et al. Light-induced engagement of microglia to focally remodel synapses in the adult brain. *Elife*, 9. (2020).
48. Spiller, K. J. et al. Microglia-mediated recovery from ALS-relevant motor neuron degeneration in a mouse model of TDP-43 proteinopathy. *Nat. Neurosci.* **21** (3), 329–340 (2018).
49. Klunk, W. E. et al. Imaging abeta plaques in living transgenic mice with multiphoton microscopy and methoxy-X04, a systemically administered Congo red derivative. *J. Neuropathol. Exp. Neurol.* **61** (9), 797–805 (2002).
50. Burgold, S. et al. In vivo multiphoton imaging reveals gradual growth of newborn amyloid plaques over weeks. *Acta Neuropathol.* **121** (3), 327–335 (2011).

51. Berg, S. et al. Ilastik: interactive machine learning for (bio)image analysis. *Nat. Methods*. **16** (12), 1226–1232 (2019).
52. Whitelaw, B. S., Matei, E. K. & Majewska, A. K. Phosphoinositide-3-Kinase gamma is not a predominant regulator of ATP-dependent directed microglial process motility or experience-dependent ocular dominance plasticity. *eNeuro*, **7**(6). (2020).

Acknowledgements
We thank the Wang lab for the interim usage of their 2-photon microscope for image acquisition. This research was supported by the Alzheimer's Association AARG-NTF-19-619116 (AKM), University of Rochester Medical Center's Del Monte Institute for Neuroscience Pilot Program (AKM, KO), a University of Rochester Goodman award (LL), and an AD supplement to NIH R01 NS114480 (AKM).

Author contributions
LHDL conceived the study in consultation with AKM and MKO. LHDL designed, conducted, and carried out data analyses for all the experiments in this study. LHDL and AKM wrote the first draft of the manuscript. All authors reviewed and contributed to the final version.

Declarations

Competing interests
The authors declare no competing interests.

Additional information
Supplementary Information The online version contains supplementary material available at https://doi.org/10.1038/s41598-024-81910-0.

Correspondence and requests for materials should be addressed to A.K.M.

Reprints and permissions information is available at www.nature.com/reprints.

Publisher's note Springer Nature remains neutral with regard to jurisdictional claims in published maps and institutional affiliations.